Nanoscale

PAPER

View Article Online
View Journal

Cite this: DOI: 10.1039/c5nr01403d

Functionalization of graphene oxide nanostructures improves photoluminescence and facilitates their use as optical probes in preclinical imaging†

Neeraj Prabhakar,[a,b,c] Tuomas Näreoja,*[b] Eva von Haartman,[a,c] Didem Şen Karaman,[a,c] Sergey A. Burikov,[d] Tatiana A. Dolenko,[d] Takahiro Deguchi,[b] Veronika Mamaeva,[e] Pekka E. Hänninen,[b] Igor I. Vlasov,[f,g] Olga A. Shenderova[h] and Jessica M. Rosenholm*[a,c]

Recently reported photoluminescent nanographene oxides (nGOs), *i.e.* nanographene oxidised with a sulfuric/nitric acid mixture (SNOx method), have tuneable photoluminescence and are scalable, simple and fast to produce optical probes. This material belongs to the vast class of photoluminescent carbon nanostructures, including carbon dots, nanodiamonds (NDs), graphene quantum dots (GQDs), all of which demonstrate a variety of properties that are attractive for biomedical imaging such as low toxicity and stable photoluminescence. In this study, the nGOs were organically surface-modified with poly(ethylene glycol)–poly(ethylene imine) (PEG–PEI) copolymers tagged with folic acid as the affinity ligand for cancer cells expressing folate receptors. The functionalization enhanced both the cellular uptake and quantum efficiency of the photoluminescence as compared to non-modified nGOs. The nGOs exhibited an excitation dependent photoluminescence that facilitated their detection with a wide range of microscope configurations. The functionalized nGOs were non-toxic, they were retained in the stained cell population over a period of 8 days and they were distributed equally between daughter cells. We have evaluated their applicability in *in vitro* and *in vivo* (chicken embryo CAM) models to visualize and track migratory cancer cells. The good biocompatibility and easy detection of the functionalized nGOs suggest that they could address the limitations faced with quantum dots and organic fluorophores in long-term *in vivo* biomedical imaging.

Received 3rd March 2015,
Accepted 30th April 2015

DOI: 10.1039/c5nr01403d

www.rsc.org/nanoscale

1. Introduction

Carbon nanostructures have emerged as a novel family of nanomaterials with biomedical prospects[1–3] especially due to their unique optical properties that have ascribed them with potential to replace currently used nanostructured imaging probes such as quantum dots (QDs).[4,5] Composed of the major element of life, carbon, these materials are thus associated with lower toxicity than their heavy metal-composed semiconductor counterparts.[6] There are several categories of carbon-based luminescent nanoparticles, such as soot, activated carbons, graphite, carbohydrates[7,8] nanotubes, and nanodiamonds[9] that have been used as precursors to luminescent carbon-based nanomaterials using oxidizing conditions at elevated temperatures. Nano-graphene oxide nanoparticles are a group of fluorescent carbon-based structures that are related to graphene oxide (GO). The atomic structure of GO is comprised of a graphene basal plane with a non-uniform coverage of oxygen-containing functional groups, such as epoxy and hydroxyl groups, resulting in sp^2 carbon islands of a few nanometers in size isolated within a defective sp^3 carbon network.[10] Edges of the GO can contain various other oxygen-containing groups.[7,9]Typical C : O ratios in GO range between 2 and 4. While luminescent GO structures can be relatively

[a]*Pharmaceutical Sciences Laboratory, Faculty of Science and Engineering, Åbo Akademi University, 20520 Turku, Finland. E-mail: jerosenh@abo.fi*
[b]*Laboratory of Biophysics, Faculty of Medicine, University of Turku, FI-20520 Turku, Finland. E-mail: tuonar@utu.fi*
[c]*Laboratory of Physical Chemistry, Faculty of Science and Engineering, Åbo Akademi University, 20500 Turku, Finland*
[d]*Department of Physics, Lomonosov Moscow State University, 119991 Moscow, Russia*
[e]*Section for Haematology, Clinical Institute 2, University of Bergen, 5020 Bergen, Norway*
[f]*General Physics Institute, Russian Academy of Sciences, 119991 Moscow, Russia*
[g]*National Research Nuclear University MEPhI, Moscow 115409, Russia*
[h]*International Technology Center, Raleigh, North Carolina, USA*
†Electronic supplementary information (ESI) available. See DOI: 10.1039/c5nr01403d

large, isolated structures of nanometer size can also be produced (nGO).[11,12] A popular method for the production of photoluminescent GO-based structures is the creation of nano-sized sp^2 islands by a partial reduction of graphite oxide. The latter is typically obtained by oxidizing graphite under harsh conditions, followed by exfoliation into predominantly single-layered sheets. The fluorescence of GO-based structures has been reported from the visible to the NIR range, and the maximum intensity is located between 500 and 800 nm.[13,14] Photoluminescence in GO-based structures was proposed to originate from emissive electronic transitions within a band gap formed by quantum confinement in the isolated sp^2 carbon islands, as well as by functionalized surface defect sites.[13,14] While nGO particles demonstrate bright stable luminescence, photoluminescent (PL) nanocarbons obtained by different chemical treatments vary widely in structure and composition as well as their PL properties.

In this study, we have used nano-graphite/graphene oxide (nGO) synthesized by oxidizing micro- and/or nanographite in a 3 : 1 sulfuric to nitric acid mixture (SNOx). Recently, we demonstrated that the SNOx method can be used to produce PL carbon nanostructures by oxidation of micrographite, nanographite and other graphitic source materials at temperatures exceeding 100 °C.[15,16] This acid mixture functions as an exceptional graphite intercalation compound which facilitates cleavage and oxidation initially forming graphite oxide followed by graphene oxide produced by exfoliation. It was possible to tune the PL emission of the reaction suspension from blue to red by tuning the combination of reaction temperature and time. Peng *et al.* showed that this mixture can oxidize carbon fibers[17] and that increasing the reaction temperature causes a blue-shift of the PL emission wavelength. The advantages of using the SNOx method for the production of nGO include scalability, simplicity and fast production time.[16]

Here, the use of photoluminescent nGO produced by the SNOx method in biomedical imaging was demonstrated both *in vivo* and *in vitro* as well as was spectrophotometrically evaluated for its excitation wavelength-dependent photoluminescent nature. To further expand the applicability of the inorganic nGOs, they were organically modified in order to (1) increase the colloidal stability in the complex physiological environment, (2) promote the cellular uptake by adding functional coatings interacting with the cell membrane, and (3) enhance the specific affinity towards cancer cells by surface-anchoring of targeting ligands.[18] We utilized folic acid (FA) as the affinity ligand, which was covalently coupled to the poly(ethylene imine)–poly(ethylene glycol) copolymer[19] and subsequently coated onto the nGOs through electrostatic adsorption. We have also evaluated their potential as an *in vitro* label for cell staining and utilized their excitation dependent emission for detection.

To evaluate the potential of nGOs for labelling and subsequent detection of labelled tumor cells in an *in vivo* setting, we used the chick embryo chorioallantoic membrane (CAM) model.[20–23] The CAM model has been put forward as a preferable method to conduct short-term *in vivo* experiments in order to avoid animal trials. The CAM model is inexpensive, easy to analyse with light microscopy, robust, and it is not subject to laboratory animal legislation nor does the use of it require specialized facilities. Moreover, it is recommended as an alternate model in the 3R principle (Replacement, Reduction and Refinement of vertebrate laboratory animals) thus replacing costly and time-consuming animal experiments. CAM serves as a source of angiogenic blood vessels that in addition to nurturing developing tumors, provides an organotypic environment for tumor cell intravasation, dissemination, and vascular arrest, and is also a repository where arrested cells extravasate to form micro metastatic foci.[22,24,25] Here we show that the studied nano-graphene oxide nanoparticles show considerable potential to become a versatile, safe and long-term probe for live light microscopy utilizing the CAM model.

2. Experimental

2.1. Particle preparation and characterization

2.1.1 Starting materials. nGO was produced by oxidation of ~400 nm natural nanographite (Nanostructured & Amorphous Materials Inc., Houston, TX) in a 3 : 1 mixture of 95–98% sulphuric acid to 68% nitric acid for 2 hours. The supernatant and residue were separated by centrifugation. The acidic mixture was evaporated from the supernatant at 350 °C and the brownish residue was resuspended in DI water at a concentration of 5 mg ml^{-1}. For the synthesis of copolymers, with and without FA, an in-house procedure was applied as follows. The chemicals that were used for copolymer synthesis, poly (ethylene glycol) methyl ether (mPEG, 5000 molecular weight), polyethyleneimine (PEI, 25 000 molecular weight), hexamethylene diisocyanate (HMDI) (>99%) were supplied by Sigma Aldrich. The folic acid (FA) ligand (>97%) was purchased from Sigma. For the FA-conjugated copolymer preparation, the maleimide-PEG-OH (MW of PEG 5 kDa, mal-PEG-OH) polymer from JENKEM Technology was used as a the starting reagent. The organic solvents, anhydrous chloroform and diethyl ether, were from Riedel-de Haën and J. T. Baker, respectively. Milli-Q water (18.2 Ω) was used throughout the study. Only analytical grade chemicals were used.

2.1.2 Copolymer synthesis. The synthesis was carried out as follows: first, the mPEG reagent was activated by HMDI for further reaction with PEI. For this purpose, 1 g of mPEG was dissolved in 25 ml of $CHCl_3$ and 3.2 ml HMDI was added. The reaction was carried out at 60 °C under reflux and with stirring overnight. After the reaction, the activated mPEG polymer was collected by precipitation with the addition of diethyl ether and collected by centrifugation at 5000 rpm for 10 minutes. After collecting the activated mPEG polymer, it was dried under vacuum. As a second step of copolymer preparation, 0.6 g of activated mPEG was reacted with 0.8 g of 25 kDa PEI in 25 ml of $CHCl_3$ under the same conditions mentioned for activation of the mPEG polymer. After the reaction, the

obtained product was purified by diethyl ether and vacuum dried. The folic acid–copolymer conjugate was prepared as follows: first, 150 mg of mal-PEG-OH was dissolved in 15 ml of $CHCl_3$ and 0.482 ml HMDI was added to the reaction solution (1 : 100 molar ratio of mal-PEG-OH : HMDI). The reaction was carried out overnight at 60 °C under reflux with stirring. Then, the activated mal-PEG–HMDI polymer was purified by the addition of diethyl ether and centrifugation (5000 rpm, 10 min). As a second step, the 25 kDa PEI polymer was reacted with the activated mal-PEG–HMDI with a molar ratio of 6 : 1 (137 mg of mal-PEG–HMDI dissolved in 15 ml of $CHCl_3$ and 110 mg of PEI was added to the reaction solution) at 60 °C under reflux overnight. The product (mal-PEG–PEI) was purified and collected as mentioned above. As a third step, cysteamine-conjugated folic acid was prepared in order to react with mal-PEG–PEI. For the cysteamine conjugated folic acid (FA–Cys) preparation, FA was dissolved in DMF and activated with HATU (1-[bis(dimethylamino)methylene]-1*H*-1,2,3-triazolo-[4,5-*b*]pyridinium 3-oxid hexafluorophosphate) for 15 min (molar ratio 1 : 1) and cysteamine was also dissolved in DMF and activated with DIPEA (*N*,*N*-diisopropylethylamine) for 15 min (molar ratio 1 : 1). The reaction solutions were mixed and kept under stirring for 24 h at RT. After the reaction was complete, the FA–Cys was precipitated with a (30 : 70) acetone: diethyl ether mixture, and separated by centrifugation at 10 000 rpm for 10 min and vacuum dried. The obtained yellow powder was kept in the freezer (at −18 °C) for further usage. For FA–Cys conjugation to the copolymer, 160 mg of the mal-PEG–PEI copolymer was dissolved in 16 ml HEPES buffer and 8.8 mg of FA–Cys was also dissolved in 8 ml of HEPES buffer and the solutions were mixed and kept under stirring for 3 h at room temperature. Then, the reaction solution was dialyzed against DI water for 24 h and freeze dried. The obtained yellow powder of the FA–PEG–PEI copolymer conjugate was kept in the freezer at −18 °C for further usage.

2.1.3 Copolymer coating. The nGO structures were coated with the in-house synthesized poly(ethylene glycol)–poly(ethylene imine) (mPEG–PEI) copolymers with (Cop–FA) and without (Cop) folic acid (FA). The nGO particles were dispersed in HEPES (25 mM, pH 7.2) using ultrasonication and purified by dialysis for 24 h before surface coating. The solvent was discarded and changed to a fresh one three times during the dialysis. The nGO particles were dispersed in HEPES (25 mM, pH 7.2) using ultrasonication. The copolymers were dissolved to a concentration of 1 mg mL^{-1} in HEPES and 10–50 wt% (with respect to the nGO) was added dropwise to the nGO dispersion during ultrasonication for a final particle concentration of 1 mg mL^{-1} to find the optimal amount. The sample was stirred at RT overnight. Copolymer-coated nGO was denoted as nGO–Cop.

2.2. PL measurements of nGO suspensions

The PL of nGO (1 mg ml^{-1} in HEPES, pH 7.2) was measured on a PTI Quanta-Master spectrofluorimeter (Photon Technology International, Lawrenceville, NJ). The excitation and the emission slits were set to 5 nm. The measurements were performed in quartz cuvettes with a light path length of 1 cm. The fluorescence intensity of nGO was detected with excitation wavelengths at 405, 488 and 532 nm.

2.3. Quantum yield measurements

Excitation of PL spectra was performed by an argon laser (wavelength 488 nm, output power 350 mW) and diode lasers (wavelengths 405 nm and 532 nm). The system of registration consisted of a monochromator (Acton, grades 900 and 1800 g mm^{-1}, focal length 500 nm, spectral resolution 1 cm^{-1}) and two detectors (PMT and CCD-camera). PL spectra in the range 410–800 nm were measured by PMT in the mode of step-by-step registration. The measurements were performed in quartz cuvettes with a light path length of 1 cm. The temperature of the samples during the experiment was maintained constant equal to (22.0 ± 0.2) °C in a thermostabilized cuvette. The spectra were normalized to the power of laser radiation and to the spectrum accumulation time.

2.4. Cellular internalization, toxicity and microscopy

The cytocompatibility of nGO, nGO–Cop, nGO–Cop–FA nanoparticles was evaluated using the WST-1 cell viability assay (Roche Diagnostics). 10 000 HeLa cells per well were grown in a 96 well plate in DMEM (10% FCS, 1% amino acids, 1% penicillin–streptomycin) and incubated overnight to adhere. Then (a) pure nGO, (b) nGO–Cop, (c) nGO–Cop–FA particles were sonicated for 15 min and added to 1 ml of pre-warmed (37 °C) growth medium at three different 10-fold increasing concentrations of 1 μg, 10 μg, and 100 μg. Then, the growth medium containing particles was further sonicated for 15 min. The growth media of cells in 96 well plates were replaced with media containing three different concentrations of (a) pure nGO, (b) nGO–Cop, (c) nGO–Cop–FA. 5 μM of staurosporine (toxin) was added as a positive control, whereas negative control cells were untreated (pure cell media only). After incubating the particles for 48 h at 37 °C, 5% CO_2, 10 μl of the WST-1 cell proliferation reagent (Roche Diagnostics, Germany) was added to each well containing 100 μl of cell growth media, and the plate was again allowed to incubate for 3 h at 37 °C, 5% CO_2. After incubation, the absorbance was read at 430 nm using a Tecan Ultra microplate reader (MTX Lab Systems, Inc.). The number of viable cells was correlated with the observed absorbance from each individual sample.

2.4.1 CAM model preparation of *ex ova* culture. Fertilized chicken eggs were obtained from LSK Poultry (Turku, Finland). Eggs were placed in a rotary thermostat incubator at 37 °C at 65% relative humidity. At day 3, eggs were wiped gently with 70% ethanol with a paper towel. Eggshells were carefully cut using a rotating saw without damaging the inner membranes. The eggs' entire content was very gently transferred into a sterile weighing boat containing 5 ml of DMEM growth medium (1% penicillin–streptomycin) and ground egg shell was added to provide calcium. Weighing boats were covered from the top with Petri dishes. The weighing boats containing eggs were allowed to incubate till day 8 at 37 °C at 65% relative humidity.

2.4.2 Preparation of *in ova* culture. Fertilized chicken eggs were obtained from LSK Poultry (Turku, Finland). Eggs were placed in a rotary thermostat incubator at 37 °C at 65% relative humidity. At day 3, eggs were gently wiped with 70% ethanol with a paper towel. A small hole was made on the egg shell and then covered with Parafilm®. The eggs were allowed to develop until day 8 at 37 °C at 65% relative humidity. Before tumor implantation, the existing holes in the eggs shells were carefully opened to facilitate tumor implantation and subsequent imaging.

2.4.3 *In vivo* multiphoton imaging of implanted tumors. The experimental setup consisted of TCS SP5 MP (Multiphoton, Leica microsystems), LASAF software (Leica application suite), non-descanned detectors (NDD) and 20× dip objective. Multi-photon microscopy was performed with a Ti–sapphire femtosecond pulse laser (Chameleon Ultra, Coherent Inc, CA, USA) at 800 nm for excitation of nGO–Cop–FA implanted tumors of the live CAM membrane placed on pre-warmed gel packs at 37 °C. The emission from particles was collected using NDD detectors (NDD1) at 430–480 nm.

3. Results and discussion

3.1. Particle preparation and characterization

Nano-graphite/graphene oxide was synthesized according to our previously reported procedure by SC Hens *et al.*[16] The prepared nGO was kept in aqueous suspension at a concentration of 5 mg ml^{-1} as a stock. To potentially enhance their performance in a biological setting (*in vitro* and *in vivo*) these nGOs were also further coated with PEG–PEI copolymers *via* electrostatic adsorption[19] by titration against copolymer concentration by dynamic light scattering to find the optimal amount of copolymers to be used (Table 1). As a result of the oxidation process, the surface of nGO possesses abundant carboxylic acid (COOH) groups, which renders the nGO surface negatively charged at neutral pH (Table 1). Thus, electrostatic adsorption can be readily realized by utilizing the polycation PEI as an 'anchor' between the nGO surface and neutral PEG chains. When an optimal copolymer ratio had been found, a third nGO sample was prepared using FA–PEG–PEI copolymers, *i.e.* with FA conjugated to the terminal end of PEG (see Scheme 1) to be used as affinity ligands towards cancer cells.[26]

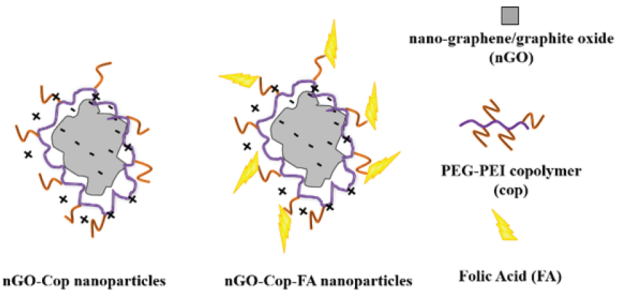

Scheme 1 Schematic representation of nGO–Cop and nGO–Cop–FA particles.

This surface coating should further enhance the colloidal stability of nGOs under biological/physiological conditions due to the electrostatic stabilization provided by PEI combined with the steric stabilization provided by PEG.[27] The dispersibility of all three resulting nGO samples (pure nGO, nGO–Cop and nGO–Cop–FA) was confirmed with dynamic light scattering (DLS) and the alteration in surface charge upon copolymer coating was followed by electrokinetic measurements (ζ-potential) (Table 1). Upon copolymer adsorption, the net surface charge at physiological pH converted from negative to positive due to the high positive charge density of PEI,[28] but was still rendered lower than that of characteristic nanoparticle surfaces functionalized with PEI only due to partial shielding (ζ-potential measured at a larger distance from the particle surface) from the PEG chains. Further, the conjugation of FA resulted in lowering of the net surface charge to slightly below zero due to the partial deprotonation of folic acid at physiological pH.[29] The morphology and size of nGO particles (nGO, nGO–Cop and nGO–Cop–FA) were studied by applying low voltage (80 kV) transmission electron microscopy (TEM) and atomic force microscopy (AFM). TEM at low magnification revealed that the nGO particles were of different sizes (Fig. S3†), but all typically below 10 nm. However, even at high magnification, it was difficult to properly investigate the particle morphology in great detail. The particles can be seen uniformly dispersed over the TEM grid (Fig. 1a). Therefore, AFM was further applied to study the size distribution. AFM shows a similar size distribution pattern (Fig. 1b) as observed by TEM. We recorded a wide distribution of sizes typically below

Table 1 Hydrodynamic size and zeta potential of pure and surface functionalized nGO

Sample	Size (number PSD)[a] [nm]	PDI	Zeta[b] [mV]
nGO	112.1 (100%)	0.287	−22.5
nGO–Cop 30 wt%	36.39 (99.7%)	0.32	13.7
nGO–Cop–FA 30 wt%	19.08 (100%)	0.34	−5.1

[a] The number size distribution was used for determining the hydrodynamic size of nGO. [b] Both DLS and electrokinetic measurements were carried out in HEPES buffer (25 mM, pH 7.2).

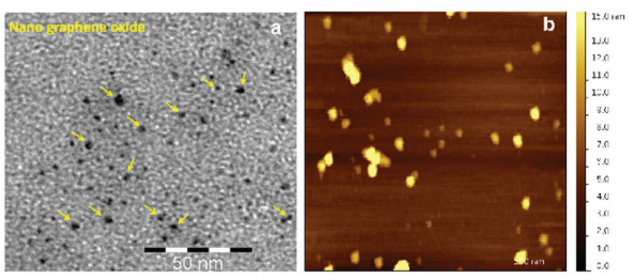

Fig. 1 Size distribution of nGOs imaged with (a) TEM and (b) AFM.

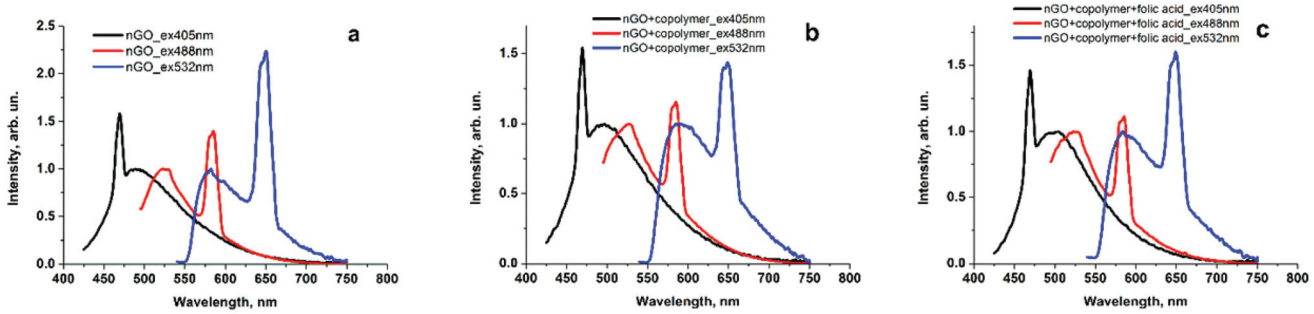

Fig. 2 PL emission spectra of pure graphene oxide nanoparticles (nGOs) showed excitation dependent emission peaks. (a) PL spectra of nGO water suspension with concentration 0.01 mg ml^{-1} under different excitation wavelengths. (b) PL spectra of, nGO–Cop water suspension with concentration 0.01 mg ml^{-1} under different excitation wavelengths. (c) PL spectra of, nGO–Cop–FA water suspension with concentration 0.01 mg ml^{-1} under different excitation wavelengths. All spectra are normalized to the fluorescence maximum.

10 nm with some larger aggregates in the nGO sample (Fig. S4†).

Nevertheless, the DLS measurements (Table 1, Fig. S1 & S2†) were performed in HEPES buffer which suggested that slight nGO aggregation may have occurred; especially for the non-polymer-coated nGO (hydrodynamic diameter >100 nm). Here, it can be seen for the plain nGO particles that they have a strong natural tendency to aggregate under these conditions. To examine the size of single particles we conducted TEM and AFM imaging of dried materials from the same stock suspension (Fig. 1). We saw a number of aggregates with uncoated nGOs and fewer with the coated materials. However, we were able to measure the sizes of a single particle's median diameters as: nGO 4.3 nm; COP 9.6 nm; COP–FA 11.1 nm (Fig. S4†). Consequently, apart from other added benefits of surface functionalization, the surface coating also efficiently prevents particle aggregation and provides colloidal stability in aqueous suspensions (Table 1).

3.2. PL properties of nGO

Excitation-dependent emission has been demonstrated by nGO over the entire visible range. GO has shown unique emission properties due to emissive electronic transitions within a band gap formed by quantum confinement in the isolated sp^2 carbon islands. To investigate this, the fluorescence properties of our nGO were characterized by the experimental setup described in section 2.3. Many different optical centres were detected, which were dependent on the excitation wavelength (Fig. 2). A systematic fluorescence spectrophotometric evaluation showed that emission maxima occur at approximately 70–90 nm from the excitation wavelength. PL spectra of water suspensions of nGO, nGO–Cop, and nGO–Cop–FA nanoparticles with the same concentration 0.01 mg ml^{-1} under excitation wavelengths 405, 488 and 532 nm are presented in Fig. 2a–c.

Comparative analysis of PL spectra of the suspensions of nGO, nGO–Cop, nGO–Cop–FA nanoparticles confirms high and stable PL properties of all three prepared suspensions. PL spectra of the water suspensions with the same concentration

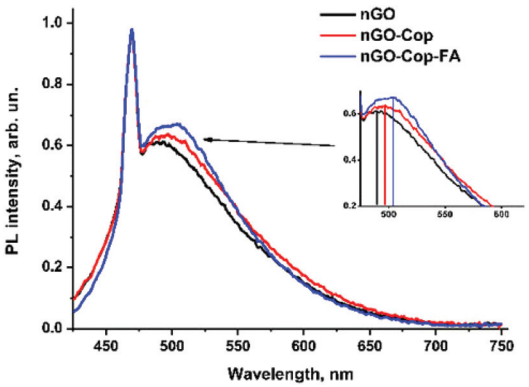

Fig. 3 PL spectra of water suspensions of nGO, nGO–Cop, nGO–Cop–FA nanoparticles with the same concentration 0.01 mg ml^{-1} (excitation wavelength 405 nm). Spectra are normalized to the maximum of the Raman water valence band. The PL maximum in the obtained spectra of water suspensions of nGO, nGO–Cop, nGO–Cop–FA moves to the "red side" by the following way: λ^{PL}_{max}(nGO) = 489 nm, λ^{PL}_{max}(nGO–Cop) = 497 nm, λ^{PL}_{max}(nGO–Cop–FA) = 504 nm. The maximum of the water Raman valence band (470 nm) does not shift. This band plays the role of the inner benchmark for our quantitative estimations of the changes of PL of nanoparticles.

0.01 mg ml^{-1} under excitation wavelength 405 nm are presented in Fig. 3.

The nanoparticle concentration above was selected so that registration of the Raman valence band of water was reliable (which was needed to calculate the F_o parameter, see below). This band was the internal reference point in the PL measurements. As can be seen from Fig. 3, coating of nGO with the copolymers (Cop and Cop–FA) does not quench PL but actually slightly increases it. The parameter F_o was used for a quantitative characterization of the PL intensities of the samples, which is the ratio of the integral intensity of fluorescence to the integral intensity of the water Raman valence band.[30] Values of F_o were determined for all the studied suspensions (Table 2). The obtained results showed that organic coating of nGO with copolymers slightly increased the PL properties. Furthermore,

Table 2 Characteristics of PL properties of nGO water suspensions

Parameters	nGO	nGO–Cop	nGO–Cop–FA
Quantum yield	4.80%	6.20%	7.10%
F_0 (λ_{exc} = 405 nm)/max_{PL}	15.8/493 nm	16.1/498 nm	17/501 nm
F_0 (λ_{exc} = 488 nm)/max_{PL}	5.3/527 nm	7.7/528 nm	8.7/528 nm
F_0 (λ_{exc} = 532 nm)/max_{PL}	3.2/588 nm	5.4/589 nm	7.6/590 nm

measurements of nGO PL spectra every day during several months showed very high fluorescence stability. All in all, the observed PL properties render all three (nGO, nGO–Cop, nGO–Cop–FA) nanoparticle formulations very promising for biomedical imaging purposes.

The graphene oxides and similar carbon structures reported in the literature have a very variable quantum efficiency, which is mainly dependent on the synthesis, functionalization and structure.[31] The latest study by Wei *et al.* demonstrated that the quantum efficiency of graphene oxide is inversely proportional to the increase in size. Typically, in the study by Wei *et al.*, the quantum efficiencies of different (graphene oxide) particle sizes of 43.5 nm, 23.1 nm and 12.3 nm were 0.83%, 2.63% and 3.73%, respectively.[31] Moreover, another study carried out by Mei *et al.* has shown that the graphene oxide quantum efficiency can be effected by the NH_2/C ratio using different alkylamine functionalizations.[32] Therefore, in our case, for our nGO produced by a different synthesis route[16] and subject to organic surface coating, it is critical to evaluate them for their PL properties. Thus, to further investigate the unique optical properties of the resulting nGO composites, a PL study was carried out after surface coating them with the organic PEG–PEI copolymers, which is a widely used strategy for organic surface modification of nanomaterials intended for biomedical applications. For inorganic nanoparticles, we have previously shown that this type of coating can promote an enhancement in cellular uptake.[19,33] The present study was intended to observe the effects of organic surface coating on the PL properties of nGOs. For water suspensions of all prepared nanoparticles, the quantum yields were measured, and these values are presented in Table 2.

Evidently, nGO particles coated by copolymers exhibited better quantum yield values than without organic coating. Consequently, the result demonstrates that organic surface modification is vital not only for appropriate colloidal stability and presumed cellular applicability, but also for enhancement of the PL properties of nGOs. The mechanism of quantum efficiency improvement by organic modification is still not properly understood, which is why more studies are required to fully understand the chemical mechanism of organic polymers in the improvement of PL properties.

3.3. Cytocompatibility

Cytotoxicity analysis is a prerequisite before any further evaluations involving biological systems. Different concentrations and surface functionalizations (in the present case, PEG–PEI copolymers and folic acid) may change the biocompatibility of a material even if it has inherently been reported as "safe". The biocompatibility of each separate surface modification of graphene oxide nanoparticles with HeLa cancer cells was thus evaluated. Staurosporine, an established kinase inhibitor cellular toxin, was used as a positive control for toxicity. The WST-1 cell viability assay was used to evaluate the cytocompatibility of all three prepared nGO suspensions at a 10-fold increasing concentration to examine the effects of both higher concentrations coupled with different surface chemistries.

The cytocompatibility evaluation showed that the pure graphene oxide (nGO) and surface-coated nGO nanoparticles even at higher concentrations are safe for cells under the experimental conditions used. The absorbance values for negative controls (cells without particles) and nGO particle-incubated cells showed equivalent viability for different surface chemical modifications. nGO-incubated cells remained highly viable after 48 h incubation in comparison with staurosporine-treated cells. The cell viability remained high even at concentrations up to 100 μg ml^{-1}. Neither upon the addition of copolymers nor on conjugation with folic acid did we observe any cytotoxicity. Previously, we found that nanocomposites based on PL nanodiamonds coated with similar copolymers were also cytocompatible.[33] The functionalization appeared to provide a small but non-significant increase in tolerability of the nGOs, possibly due to the lower tendency to form aggregates (Fig. 4). With the toxicity levels determined, all nGO variants were established to be safe and applicable for further *in vitro* and *in vivo* applications.

3.4. Cellular imaging

The optical detectability of cells labelled with nGOs *in vitro* was investigated by confocal and two-photon excitation

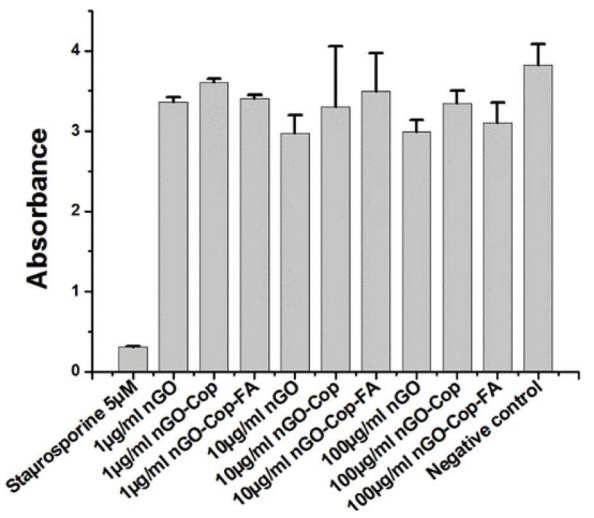

Fig. 4 Graphical representation of cell viability evaluated by the WST-1 assay. The absorbance values are directly proportional to the number of viable HeLa cells. Staurosporine (5 μM) was added to the HeLa cells as the positive control, whereas the negative control HeLa cells were untreated. 10 fold increasing particle concentrations of nGO and surface modified nGO nanoparticles were added.

microscopy. *In vitro* detectability was evaluated for HeLa, MDA-MB-231 and A549 cancer cells incubated with nGO–Cop–FA nanoparticles (ESI† Fig. S6). These three cell lines were chosen due to their different levels of overexpression of folate receptors (FRs).[34–36] The surface-functionalized nGO nanoparticles could readily be detected by confocal as well as two-photon imaging (Fig. 5a, b). The bright photoluminescence from nGO–Cop–FA was detected throughout the cells, which indicated that nGO–Cop–FA particles were efficiently internalized by the different cancer cells; and finally they were localized outside the nucleus (Fig. 5). The particles seem to be localized in endosomes, where they are collected as a result of their trafficking into these intracellular compartments after cellular uptake by endocytosis,[37] consequently forming intracellular aggregates of detectable size. Smaller nGO clusters can also be seen to spread across the entire cytoplasm, which should be a result of endosomal escape of the particles, a process which can be facilitated by the aid of PEI. The cellular uptake enhancement followed by endosomal escape facilitated by surface coating of inorganic nanoparticles with the corresponding PEG–PEI copolymers has been reported previously.[28,33,38] Here, the efficient internalization of particles imparted by the surface coating improves the overall detectability of cells, promoting the use of nGOs as cellular labels.

The HeLa cells incubated with nGO–Cop (Fig. 5b) for 6 h were excited at 960 nm and were detectable at 520–580 nm. The intracellular nGOs were mainly localized in the cytoplasm and the signal-to-noise ratio was improved for PL detection. The PL from nGOs was detectable both with the argon ion laser (488 nm) and the Ti:sapphire femtosecond pulsed laser for two-photon excitation. Our data demonstrate that the copolymer-coated nGOs could be used as a bright optical probe for *in vitro* two-photon microscopy (Fig. 5b). An excitation with near-infrared wavelength has been shown to incur less scattering, photobleaching and photodamage in *in vivo* models and deep tissue imaging.[39,40] Two-photon microscopy excites the fluorophores in a femtoliter volume axially confined at the focal plane and the longer excitation wavelengths allow deeper penetration in the specimen in tissue samples.[41] Consequently, nGOs are an attractive choice for imaging probes for two-photon microscopy and exhibit detectable, bright PL in the visible range.

3.5. Effect of surface functionalization on cellular labelling

To facilitate cellular labelling, PEG–PEI copolymers were electrostatically adsorbed on the surface of the negatively charged nGO, as this mode of action proved to be efficient for the cellular uptake of our nanodiamond-based composite structures in our previous study.[33] This resulted in a net positive charge (Table 1) induced by adsorption of highly positively charged PEI, which prospectively improves the cellular uptake by interacting with negatively charged cell membranes, whereas the PEG part of the copolymer provides colloidal stability by steric stabilization.[42]

Surface coating with PEG–PEI copolymers that had been additionally conjugated to the cancer-specific ligand FA was employed in order to maximize the affinity towards cancer cells, as FA is a generic targeting ligand for a variety of different cancers.[43–45] The intracellular intensity of nGO coated with FA–PEG–PEI copolymers (Fig. 6 and 7e) was thereafter compared to that of cells incubated with pure nGOs (Fig. 6 and 7b) suggesting that the cellular uptake of nGOs was enhanced by almost 100% by applying suitable organic modification, possibly also connected to better redispersibility of coated nanoparticles under aqueous conditions (Table 1) and especially under complex biological conditions.

3.6. Excitation dependent emission

In tracking applications where several fluorescent reporters are employed, compromises typically need to be made between optimal sensitivity and spectral overlap of different labels. nGO has attractive photoluminescence properties because its

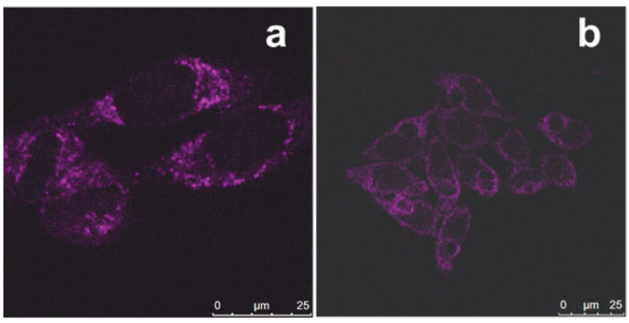

Fig. 5 PL images from fixed HeLa cells incubated with 10 µg ml^{-1} nGO–Cop–FA for 7 h. (a) HeLa cells, (b) two-photon imaging of HeLa cells incubated for 6 h with 10 µg ml^{-1} nGO–Cop. Confocal imaging: argon laser Ex. 488 nm, Em. 520–580 nm. MP imaging: Ti:sapphire (Mai Tai HP, Newport) femtosecond pulse laser Ex. 960, Em. 520–580 nm.

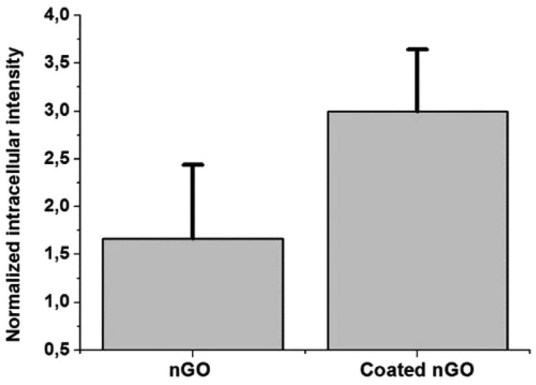

Fig. 6 Surface coating (PEG–PEI copolymers, Cop) with affinity ligands (FA) improves cellular uptake and detectability in HeLa cells. HeLa cells were incubated with 10 µg ml^{-1} of nGO and nGO–Cop–FA for 24 h. Both the respective samples were imaged with a confocal microscope using constant setting (argon laser Ex. 488 nm, Em. 528–630 nm). The intracellular intensity due to particle uptake in the cells was measured and compared by ImageJ based intensity analysis. Error bars represent intensity variation among the individual sample.

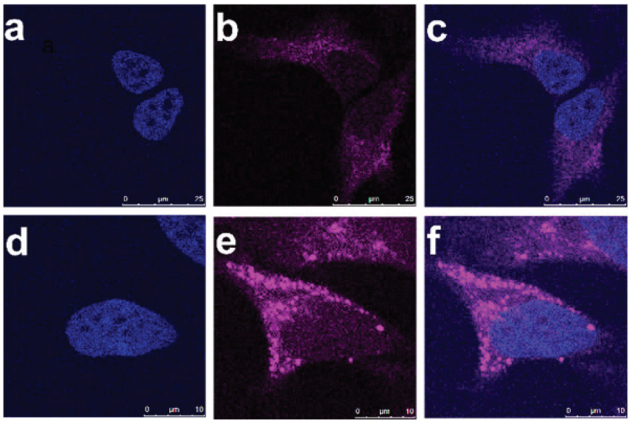

Fig. 7 (a) Nuclei stained with Hoescht dye (b) PL from pure nGO particles (c) overlay. The surface functionalization with copolymer improves uptake and quantum efficiency of nGO particles and thus increases the detectability of cells. (d) Hoescht nuclear dye (e) enhanced cellular uptake can be seen in cells (f) overlay images. Confocal imaging: argon laser Ex. 488 nm, Em. 528–630 nm. MP imaging (Hoescht): Ti:sapphire (Mai Tai HP, Newport) femtosecond pulse laser Ex. 740, Em. blue wavelength range.

excitation is dependent on emission, thus allowing emission in the entire visible wavelength range.[46] To investigate if the multicolour emission properties were retained also upon cellular labelling with the nGO, the nGO–Cop–FA incubated HeLa cells were fixed and imaged with different excitation wavelengths (argon laser lines 458 nm, 488 nm, 514 nm and HeNe diode laser 633 nm) and they were collected in a narrow detection range to allocate real RGB colors (Fig. 8).

As can be seen in Fig. 8, PL from nGOs can be efficiently collected in a colour specific manner using a narrow bandwidth of wavelengths. nGOs might thus offer great potential to use a combination of different fluorophores for imaging by using a constant nGO excitation and emission. This can be validated in Fig. 8, where Hoechst nuclear stained cells were constantly excited by a femtosecond MP laser, whereas nGO emission and excitation were varied. Therefore, unique emission properties of nGO allow it to be used with different existing cellular stains. nGO emission in the far red region is especially attractive to be exploited for *in vivo* imaging applications with different animal models.[47,48] Application of the giant red-edge effect has thus far been non-existent, but the most obvious use of the phenomenon would be fluorescence wavelength tuning *in situ* by simply changing the excitation wavelength. This feature of nGO has now been presented in multiplexed *in vivo* imaging setup where optimal contrast can be tuned in relation to the other stain sample to provide the optimal contrast for each staining. Another practical use of nGOs in biological sensing as tuneable full spectrum fluorescent light sources would be the application of a single laser line to excite two labels with a single exposure, thus essentially doubling the image acquisition speed and limiting the phototoxicity effects caused by excitation.

3.7. nGO distribution in daughter cells

Confocal imaging of dividing HeLa cells revealed that nGOs were distributed evenly among the daughter cells (Fig. 9). This further implies that nGOs could be used for cellular detection for longer periods of time. Long term tracking or detection is important to address a range of quantitative cellular behaviours such as cell migration, cell division and apoptosis.

Consequently, nGO acts as a stable and non-toxic marker that remains localized in cells upon successive cell divisions. It can be detected in dividing cells and is detectable upon successive divisions till 1 week during the *in vivo* experiments (below). Cell labelling with nGO does not show any apparent effect on cellular functions such as division and proliferation. Therefore, nGO could be applied for long-term detection and tracking of primary cells in 3D *in vitro* cultures or in *in vivo* xenografts for events such as cancer cell metastasis.[49]

3.8. CAM model

The *ex ova* version of the CAM model was chosen to be a model for *in vivo* imaging. The *ex ova* model offers large surface area, easy access to microvasculature and implantation of nGO–Cop–FA labelled tumor cells.[22,50] Cancer cell lines (HeLa, intermediate FR; MDA-MB-231, high FR; and, A549 low FR) were incubated for 24 h with the nGO–Cop–FA particles as cellular labels and implanted on the CAM on the 8th day. The

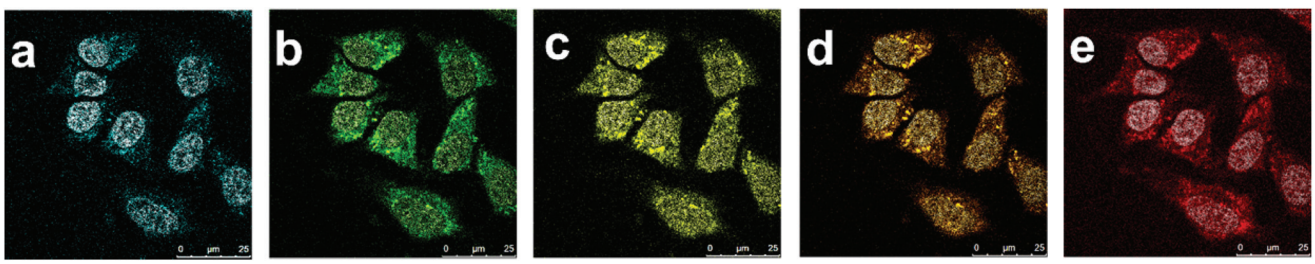

Fig. 8 (a) Different argon laser excitation at 458 nm, 488 nm, 514 nm, 633 nm was used for nGO–Cop incubated cells. Emission from particles was collected at (a) 470–500 nm for excitation at 458 nm, (b) 528–558 nm for excitation at 488 nm, (c) 558–588 nm for excitation at 488 nm, (d) 584–618 nm for excitation at 514 nm and (e) 649–703 nm for excitation at 633 nm. MP imaging (Hoescht): Ti:sapphire (Mai Tai HP, Newport) femtosecond pulse laser Ex. 740, Em. blue wavelength range.

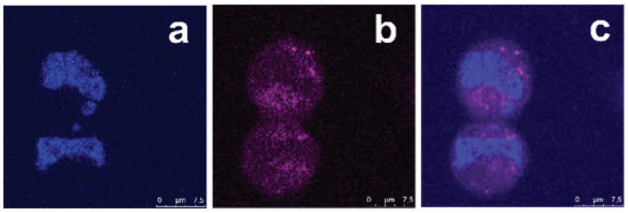

Fig. 9 Equivalent distribution of graphene oxide nanoparticles (nGO) among dividing daughter cells. Both the daughter cells contain nGO upon division. (a) Hoechst stained nucleus, (b) daughter cells carrying nGO and (c) overlay.

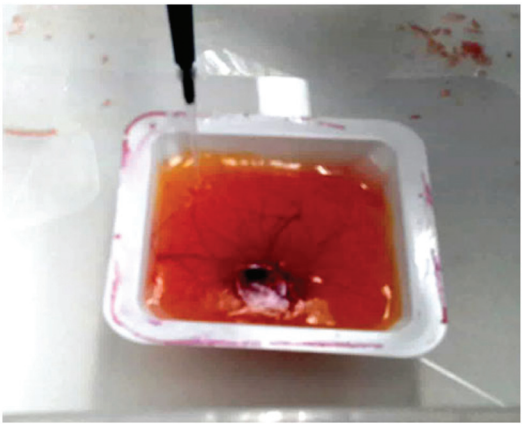

Fig. 10 Shell-less (*ex ova*) egg in cell media containing weighing boats. Implantation of 10 μg ml^{-1} nGO–Cop–FA labelled tumors over a highly vascularized CAM at day 8.

model was allowed to continue to grow under clean and light restricted conditions (Fig. 10).

Vascularized tumors from HeLa, MDA-MB-231 and A549 cancer cell lines were successfully grown on CAM and intravascularization of implanted cancer cells was also observed by adhesion to other foci on CAM.

3.9. Multiphoton *in vivo* imaging of nGO labeled tumors

To demonstrate nGO–Cop–FA's applicability in a preclinical setting, we recorded invasion of nGO–Cop–FA labelled tumors on both *in ova* and *ex ova* CAM models by two-photon imaging (Fig. 11). nGO–Cop–FA-labelled HeLa, MDA-MB-231 and A549 cancer cells expressing folate receptors[34] were implanted over CAM and allowed to form tumors over a one week time period, whereafter they were imaged on a multiphoton microscope with the excitation wavelength at 800 nm, and emission was detected at 430–480 nm. Employing two-photon imaging successfully circumvented the typical interference from autofluorescence of biological materials at this wavelength range. The nGO–Cop–FA labelled cancer cells (Fig. 11a–c) were detectable with two-photon imaging after 1 week of tumor implantation. The CAM model thus provided technical simplicity, an *in vivo* environment and it was an especially suitable animal model for optical *in vivo* imaging in sub-cellular resolution. Imaging of nGO labelled tumors over CAM with multiphoton microscopy allowed deep tissue penetration, low amount of photodamage to the tumors and enhanced contrast for live imaging (Fig. 11a–c).

The cancer cell labelling with nGO–Cop–FA particles for 24 h incubation *in vitro* at a concentration of 10 μg ml^{-1} was sufficient to detect them over CAM after the 8^{th} day of implantation. The photoluminescence from the nGOs was a strong enough image of the circulating and arrested cancer cells in the dynamic environment of the live CAM model (ESI† Movie S7). The cells remained viable as the non-toxic nature of nGO made them suitable for long term imaging even after 1 week of implantation, after which the chick development had to be terminated according to the standard CAM model procedure. The nGO-labelled implanted tumors were imaged a number of times over the 1 week period; by using low laser power we were able to avoid noticeable damage to the implanted cells/tumors or blood vessels of the live embryo. In the field of personalized oncology there is a growing need for cellular staining that would have minimal impact on tumor biology and

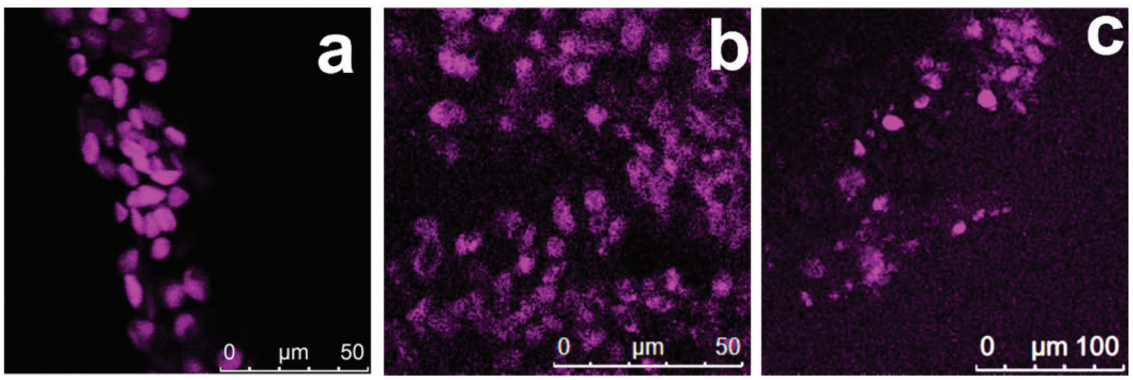

Fig. 11 Graphene oxide as an optical agent for *in vivo* imaging of tumors. Different cancer cells incubated with nGO–Cop–FA implanted on CAM for *in vivo* detection (a) HeLa cells, (b) A459 cells, (c) MDA-MB-231 cells after one week of implantation, allowing tumors to form. [MP Ex. 800 nm, non descanned detector Em. 430–480 nm, 20× dip objective].

could be applied on primary cells to be examined in 3D cultures and *in vivo* xenografts. These results demonstrate the potential of nGO as an optical probe for non-invasive *in vivo* imaging.

4. Conclusion

In this work, we have comprehensively studied a novel type of nGO to realize its potential for biomedical applications. We have successfully coated the nGO nanoparticles with organic copolymers, with or without the cancer-specific affinity ligand folic acid, to increase the biomedical applicability of nGO with a special focus on cellular labelling for *in vivo* cancer imaging using a very optically transparent and ethical animal model, the CAM model. The organic coating was shown to enhance the performance of nGO in a biological setting in a number of ways: improved dispersibility under aqueous conditions, increased quantum yield as well as enhanced cellular labelling efficiency in cancer cells with improved cellular detectability as a result. The PL properties of nGOs were characterized using laser spectrometry in a standard confocal setup and in non-linear two-photon microscopy that is an especially facilitative biomedical imaging technique for *in vivo* imaging. The spectra were measured in a physiological environment and in a standard LSCM-setup to demonstrate the wide applicability of nGO as nano-sized labels. The nGOs, functionalized or not, were shown to be safe during *in vitro* studies and as a material assured biocompatibility for *in vivo* detection of cancer cells. The nGOs were readily taken up due to their small size, they can be labelled over a single passage, they distribute evenly between daughter cells and are non-toxic so they can be labelled in quantities sufficient to monitor the tumor growth over several weeks. In conclusion, we have explored and demonstrated their applicability in tracking of cell populations in an *in vivo* model to establish them as biocompatible, non-invasive and photostable optical labels with broad versatility that can be utilized in conjunction with any other label due to their wide and tuneable PL emission properties.

Acknowledgements

The authors would like to acknowledge LSK Poultry Oy, 23800 Laitila, Finland, Dr Shishir Jaikishan, Prof. J. Peter Slotte, Helena Saarento, Jari Korhonen, Senthil Kumar Rajendran, Markus Peurla and Laboratory of Electron Microscopy, University of Turku, Finland. Financial contribution from Academy of Finland projects #137101 (NP, EvH, JMR) #140193 & 278812 (JMR) #260599 (NP, EvH, DSK, VM, JMR) #126998 (TN and PEH), from Russian Foundation for Basic Research project #15-29-01290 (TAD, SAB and IIV), Russian Academy of Sciences Program #1 (TAD, SAB and IIV) and the Doctoral Education Network in Materials Research at Åbo Akademi University (NP) and Graduate School iBioMEP (TD) are greatly acknowledged.

Notes and references

1 S. C. Ray, A. Saha, N. R. Jana and R. Sarkar, *J. Phys. Chem. C*, 2009, **113**, 18546–18551.
2 S. Chandra, P. Das, S. Bag, D. Laha and P. Pramanik, *Nanoscale*, 2011, **3**, 1533.
3 P. Juzenas, A. Kleinauskas, P. G. Luo and Y.-P. Sun, *Appl. Phys. Lett.*, 2013, **103**, 063701.
4 T. S. Hauck, R. E. Anderson, H. C. Fischer, S. Newbigging and W. C. W. Chan, *Small*, 2010, **6**, 138–144.
5 S. N. Baker and G. A. Baker, *Angew. Chem., Int. Ed.*, 2010, **49**, 6726–6744.
6 S.-T. Yang, X. Wang, H. Wang, F. Lu, P. G. Luo, L. Cao, M. J. Meziani, J.-H. Liu, Y. Liu, M. Chen, Y. Huang and Y.-P. Sun, *J. Phys. Chem. C*, 2009, **113**, 18110–18114.
7 J.-H. Liu, S.-T. Yang, X.-X. Chen and H. Wang, *Curr. Drug Metab.*, 2012, **13**, 1046–1056.
8 L. Cao, M. J. Meziani, S. Sahu and Y.-P. Sun, *Acc. Chem. Res.*, 2013, **46**, 171–180.
9 X. Zhang, S. Wang, C. Zhu, M. Liu, Y. Ji, L. Feng, L. Tao and Y. Wei, *J. Colloid Interface Sci.*, 2013, **397**, 39–44.
10 S. Zhu, S. Tang, J. Zhang and B. Yang, *Chem. Commun.*, 2012, **48**, 4527–4539.
11 X. Sun, Z. Liu, K. Welsher, J. T. Robinson, A. Goodwin, S. Zaric and H. Dai, *Nano Res.*, 2008, **1**, 203–212.
12 G. Eda, Y.-Y. Lin, C. Mattevi, H. Yamaguchi, H.-A. Chen, I.-S. Chen, C.-W. Chen and M. Chhowalla, *Adv. Mater.*, 2010, **22**, 505–509.
13 J. Shen, Y. Zhu, C. Chen, X. Yang and C. Li, *Chem. Commun.*, 2011, **47**, 2580–2582.
14 C. Galande, A. D. Mohite, A. V. Naumov, W. Gao, L. Ci, A. Ajayan, H. Gao, A. Srivastava, R. B. Weisman and P. M. Ajayan, *Sci. Rep.*, 2011, **1**, 85.
15 S. C. Hens, G. Cunningham, G. McGuire and O. Shenderova, *Nanosci. Nanotechnol. Lett.*, 2011, **3**, 75–82.
16 S. Ciftan Hens, W. G. Lawrence, A. S. Kumbhar and O. Shenderova, *J. Phys. Chem. C*, 2012, **116**, 20015–20022.
17 J. Peng, W. Gao, B. K. Gupta, Z. Liu, R. Romero-Aburto, L. Ge, L. Song, L. B. Alemany, X. Zhan, G. Gao, S. A. Vithayathil, B. A. Kaipparettu, A. A. Marti, T. Hayashi, J.-J. Zhu and P. M. Ajayan, *Nano Lett.*, 2012, **12**, 844–849.
18 J. M. Rosenholm, A. Meinander, E. Peuhu, R. Niemi, J. E. Eriksson, C. Sahlgren and M. Lindén, *ACS Nano*, 2009, **3**, 197–206.
19 D. Şen Karaman, T. Gulin-Sarfraz, G. Hedström, A. Duchanoy, P. Eklund and J. M. Rosenholm, *J. Colloid Interface Sci.*, 2014, **418**, 300–310.
20 J. Azzarello, M. A. Ihnat, B. P. Kropp, L. A. Warnke and H.-K. Lin, *Biomed. Mater.*, 2007, **2**, 55.
21 X. Liu, X. Wang, A. Horii, X. Wang, L. Qiao, S. Zhang and F.-Z. Cui, *Nanoscale*, 2012, **4**, 2720–2727.
22 E. I. Deryugina and J. P. Quigley, *Histochem. Cell Biol.*, 2008, **130**, 1119–1130.
23 A. Chwalibog, E. Sawosz, S. Jaworski, M. Kutwin, A. Hotowy, M. Wierzbicki, M. Grodzik, N. Kurantowicz, B. Strojny and L. Lipinska, *Int. J. Nanomed.*, 2014, 3913.

24 R. Auerbach, R. Lewis, B. Shinners, L. Kubai and N. Akhtar, *Clin. Chem.*, 2003, **49**, 32–40.
25 R. Auerbach, L. Kubai, D. Knighton and J. Folkman, *Dev. Biol.*, 1974, **41**, 391–394.
26 A. Garcia-Bennett, M. Nees and B. Fadeel, *Biochem. Pharmacol.*, 2011, **81**, 976–984.
27 R. Gref, A. Domb, P. Quellec, T. Blunk, R. H. Müller, J. M. Verbavatz and R. Langer, *Adv. Drug Delivery Rev.*, 1995, **16**, 215–233.
28 O. Boussif, F. Lezoualc'h, M. A. Zanta, M. D. Mergny, D. Scherman, B. Demeneix and J. P. Behr, *Proc. Natl. Acad. Sci. U. S. A.*, 1995, **92**, 7297–7301.
29 L. Bergman, J. Rosenholm, A.-B. Öst, A. Duchanoy, P. Kankaanpää, J. Heino and M. Lindén, *J. Nanomater.*, 2008, **2008**, 51:1–51:9.
30 T. A. Dolenko, S. A. Burikov, J. M. Rosenholm, O. A. Shenderova and I. I. Vlasov, *J. Phys. Chem. C*, 2012, **116**, 24314–24319.
31 J. Wei, J. Qiu, L. Ren, K. Zhang, S. Wang and B. Weeks, *Sci. Adv. Mater.*, 2014, **6**, 1052–1059.
32 Q. Mei, K. Zhang, G. Guan, B. Liu, S. Wang and Z. Zhang, *Chem. Commun.*, 2010, **46**, 7319–7321.
33 N. Prabhakar, T. Näreoja, E. von Haartman, D. Ș. Karaman, H. Jiang, S. Koho, T. A. Dolenko, P. E. Hänninen, D. I. Vlasov, V. G. Ralchenko, S. Hosomi, I. I. Vlasov, C. Sahlgren and J. M. Rosenholm, *Nanoscale*, 2013, **5**, 3713–3722.
34 R. Senthilkumar, D. Ș. Karaman, P. Paul, E. M. Björk, M. Odén, J. E. Eriksson and J. M. Rosenholm, *Biomater. Sci.*, 2014, **3**, 103.
35 R. Meier, T. D. Henning, S. Boddington, S. Tavri, S. Arora, G. Piontek, M. Rudelius, C. Corot and H. E. Daldrup-Link, *Radiology*, 2010, **255**, 527–535.
36 M. García-Díaz, S. Nonell, A. Villanueva, J. C. Stockert, M. Cañete, A. Casadó, M. Mora and M. L. Sagristá, *Biochim. Biophys. Acta*, 2011, **1808**, 1063–1071.
37 T.-G. Iversen, T. Skotland and K. Sandvig, *Nano Today*, 2011, **6**, 176–185.
38 L. Feng, X. Yang, X. Shi, X. Tan, R. Peng, J. Wang and Z. Liu, *Small Weinh. Bergstr. Ger.*, 2013, **9**, 1989–1997.
39 F. Helmchen and W. Denk, *Nat. Methods*, 2005, **2**, 932–940.
40 K. Svoboda and S. M. Block, *Annu. Rev. Biophys. Biomol. Struct.*, 1994, **23**, 247–285.
41 M. Rubart, *Circ. Res.*, 2004, **95**, 1154–1166.
42 R. A. Sperling and W. J. Parak, *Philos. Trans. R. Soc. A: Math. Phys. Eng. Sci.*, 2010, **368**, 1333–1383.
43 A. R. Hilgenbrink and P. S. Low, *J. Pharm. Sci.*, 2005, **94**, 2135–2146.
44 C. M. Paulos, J. A. Reddy, C. P. Leamon, M. J. Turk and P. S. Low, *Mol. Pharmacol.*, 2004, **66**, 1406–1414.
45 S. A. Kularatne and P. S. Low, *Methods Mol. Biol.*, 2010, **624**, 249–265.
46 N. Puvvada, B. N. P. Kumar, S. Konar, H. Kalita, M. Mandal and A. Pathak, *Sci. Technol. Adv. Mater.*, 2012, **13**, 045008.
47 B. W. Rice, M. D. Cable and M. B. Nelson, *J. Biomed. Opt.*, 2001, **6**, 432–440.
48 S. Tanaka and S. Kizaka-Kondoh, *Gan To Kagaku Ryoho*, 2008, **35**, 1272–1276.
49 E. B. Voura, J. K. Jaiswal, H. Mattoussi and S. M. Simon, *Nat. Med.*, 2004, **10**, 993–998.
50 N. A. Lokman, A. S. F. Elder, C. Ricciardelli and M. K. Oehler, *Int. J. Mol. Sci.*, 2012, **13**, 9959–9970.